Publishing House
AKAPIT

COMPUTER METHODS IN MATERIALS SCIENCE

Informatyka w Technologii Materiałów

Vol. 10, 2010, No. 4

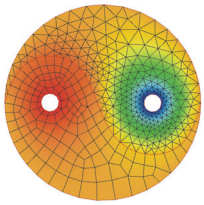

PREDICTION OF STATICALLY RECRYSTALLIZED MICROSTRUCTURE DURING EXTRUSION OF ALUMINUM ALLOYS

PETER CVAHTE[1], GORAN KUGLER[2], TOMAŽ RODIČ[2]*

[1] Impol 2000 d.d., Partizanska 38, 2310 Slovenska Bistrica, Slovenia
[2] Faculty of Natural Sciences and Engineering University of Ljubljana, Askerceva 12, 1000 Ljubljana, Slovenia
**Corresponding author: Tomaz.Rodic@ntf.uni-lj.si*

Abstract

To predict evolution of microstructure of aluminum alloys after deformation a numerical model based on the method of cellular automata (CA) has been developed and combined with the finite element model (FEM). The main objective of the combined FEM-CA model is to enable numerical predictions of growth of grains in the subsurface layers of extruded bars that occurs after deformation before the quenching in the industrial hot extrusion production chain. The results of numerical simulations show a good agreement with the results of optical micrographs of the bars taken from the industrial experiments. The outcomes of this research demonstrate that numerical models can be successfully applied to simulate complex thermo-mechanical and metallurgical processes during hot extrusion.

Key words: hot working, extrusion, static recrystallization, finite element method, cellular automata

1. INTRODUCTION

Modern industrial production of extruded aluminum profiles generally consist of series of metallurgical operations. The processing chain usually starts with the preparation of a melt and casting, which is followed by homogenization of the material and its cooling with prescribed cooling rate. During the hot extrusion cast and homogenized microstructure is deformed and hot workability of the material is strongly influenced by the thermal history of the material. The microstructure evolution and consequently the final properties of the extruded profiles are strongly influenced by the extrusion parameters such as extrusion ratio, ram speed, temperatures of the billet container and die, quality of the tool surface, extrusion mode and cooling conditions after hot deformation (Sheppard, 1999). When planning the production process these parameters should be carefully selected in order to obtain uniform microstructure through cross-section and along the profile length, and the surface without imperfections. Namely it is well-known that during hot extrusion of aluminum alloys, the extrusion parameters influence subsequent surface recrystallization which can result in undesirable appearance of coarse grains within the surface zone (Peng & Sheppard, 2004). The production of profiles without such surface zone is expensive since it requires higher homogenization temperature, high cooling rate after homogenization, fast heating and higher hot working temperature, low extrusion rate and fast quenching after extrusion. But in some cases thin surface zone with thickness usually prescribed by the customer is tolerated. In

 ISSN 1641-8581

industry, obtaining the appropriate parameters is traditionally based on practical experience of engineers and trial and error procedure, which can be very expensive. On the other hand rapid development of numerical models in recent years can assist optimization of processing parameters and hence help to reduce the costs.

The aim of the present contribution is to develop a simple model for the real industrial process that enables simulations of hot extrusion and prediction of spatial evolution of microstructure during static recrystallization which occurs after deformation. The influence of thermomechanical processing parameters, e.g. strain rate and temperature on the flow stress has been determined by laboratory testing. The industrial measurements in the real production process have been conducted and microstructures of the produced profiles have been systematically examined by microscopy. Based on the results of laboratory testing and industrial measurements a macroscopic FEM model for simulations of hot extrusion was developed and coupled with mesoscopic model based on CA method for simulations of static recrystallization after hot extrusion.

2. EXPERIMENTAL

2.1. Material and experimental procedure

For the present investigation AA6262 aluminum alloy with chemical composition given in table 1 was casted into bars with ϕ282 using AirSlip® billet casting technology. Casted bars have been cut into billets of length of 1450 mm and homogenized for 6 hours at 480°C. After homogenization they have been cooled with water employing cooling rate of ~4K/s.

Table 1. *Chemical composition of the alloy AA6262 in wt. %. (Spectrolab LAB LAVMC07A)*

Si	Fe	Cu	Mn	Mg	Cr	Zn	Ti	Pb	Bi	Al
0.744	0.4682	0.2832	0.1065	1.029	0.0593	0.0456	0.0256	0.63	0.5028	95.055

To obtain the hot working parameters for the numerical simulation of extrusion the cylindrical specimens with dimensions ϕ 10 mm x 15 mm were machined from the homogenized billet. The hot-compression tests were carried out on the Gleeble 1500D thermo-mechanical simulator. The following testing conditions were selected: temperature range 470–570°C, strain rates between 0.01 and 10s^{-1} and a true strain of 0.9. The specimens were heated to

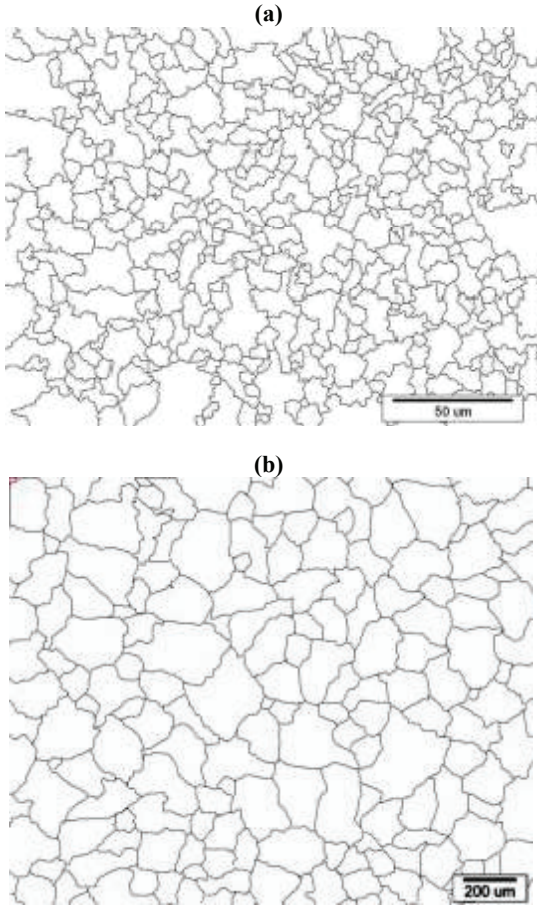

Fig. 1. *Microstructure of the AA6262 alloy obtained by optical microscopy: as cast and homogenized before extrusion with mean grain size of 64μm (a) and non-recrystallized after extrusion with mean grain size of 6μm (b).*

deformation temperature with a heating rate of 3K/s which was followed by holding them for 3 min at this temperature prior to deformation. After deformation they were water quenched. To avoid inhomogeneous deformation and sticking between the specimen and the compression tool, tantalum foil with a thickness of 0.1 mm was inserted between the cylindrical specimen and the compression anvil, and a Ni-based lubricant was used. In order to reveal the grain structure of the alloy the samples have been cut and polished which was followed by anode oxidation with HBF4 2.5% for 1.5 min at voltage of 25V. The microstructure of the alloy prior deformation is shown on figure 1a.

2.2. Hot extrusion

Homogenized billets have been extruded on 55 MN direct extrusion press using a die with 4 apertures of ϕ35mm (see figure 2). The temperature of the billets was 500°C. In order to study the influence of extrusion speed on the evolution of microstructure during static recrystallization of the regions near the surface of the extruded rods, 5 different extrusion rates were employed. Microstructure of the material after hot extrusion with speed of the ram of 9.9 mm/s taken from the center of the rod, where static recrystallization did not occurr is shown in figure 1b.

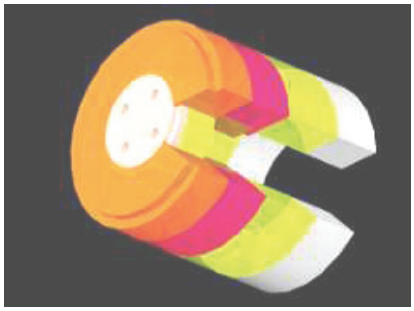

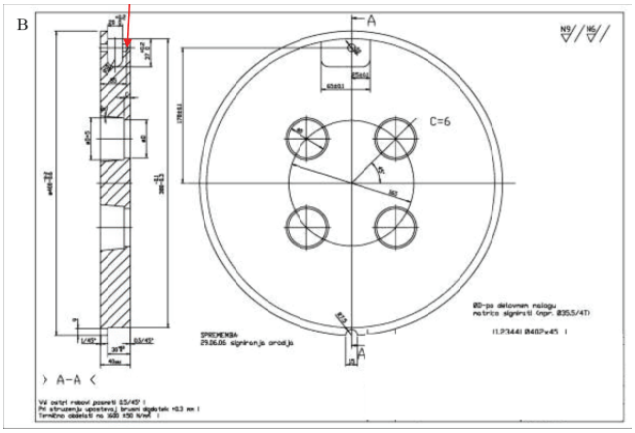

Fig. 2. *Geometry and dimensions of the extrusion tool used in industrial extrusion process and in numerical simulations.*

3. DESCRIPTION OF THE MODELS

3.1. Numerical modeling of hot extrusion process

To evaluate thermomechanical processing conditions during the extrusion of aluminium at high temperatures a finite element model has been applied where the numerical formulation takes into account coupling between transient mechanical and thermal fields. At the local level corresponding to the finite element integration points the following sets of residual equations are formulated depending whether the analysed material is assumed to be in elastic or plastic state. For elastic case the equations are

$$f(\boldsymbol{\sigma}(\boldsymbol{\varepsilon}_e^{trial}))<0 \quad \begin{cases} \boldsymbol{\Phi}=\begin{Bmatrix} \boldsymbol{\varepsilon}_p - {}^{p}\boldsymbol{\varepsilon}_p \\ d\lambda \end{Bmatrix}=0 \\ \boldsymbol{\Psi}=\begin{Bmatrix} \int_\Omega \rho c_p \dfrac{\partial T}{\partial t}\delta T\, d\Omega+\int_\Omega \nabla\delta T\cdot(k\nabla T)d\Omega-\int_\Omega q\,\delta T\, d\Omega \\ \int_\Omega \boldsymbol{\sigma}(\boldsymbol{\varepsilon}_e^{trial}):\dfrac{\partial \boldsymbol{\varepsilon}_e^{trial}}{\partial \mathbf{u}}\, d\Omega \end{Bmatrix}+\boldsymbol{\Psi}^{external}=0, \end{cases} \tag{1}$$

while for the plastic state the equations are

$$f(\boldsymbol{\sigma}(\boldsymbol{\varepsilon}_e^{trial}))\geq 0 \quad \begin{cases} \boldsymbol{\Phi}=\begin{Bmatrix} \boldsymbol{\varepsilon}_p - {}^{p}\boldsymbol{\varepsilon}_p - \lambda\dfrac{\partial f}{\partial \boldsymbol{\sigma}} \\ f(\boldsymbol{\sigma}(\boldsymbol{\varepsilon}_e^{trial})) \end{Bmatrix}=0 \\ \boldsymbol{\Psi}=\begin{Bmatrix} \int_\Omega \rho c_p \dfrac{\partial T}{\partial t}\delta T\, d\Omega+\int_\Omega \nabla\delta T\cdot(k\nabla T)d\Omega-\int_\Omega q\,\delta T\, d\Omega \\ \int_\Omega \boldsymbol{\sigma}(\boldsymbol{\varepsilon}_e^{trial}):\dfrac{\partial \boldsymbol{\varepsilon}_e^{trial}}{\partial \mathbf{u}}\, d\Omega \end{Bmatrix}+\boldsymbol{\Psi}^{external}=0. \end{cases} \tag{2}$$

In the above equations f is the yield potential, vector $\boldsymbol{\sigma}$ corresponds to the stress tensor, vector $\boldsymbol{\varepsilon}$ corresponds to the strain tensor, λ is the plastic multiplier, ρ material density, c_p specific heat capacity, T temperature, k heat conductivity, $\mathbf{u}$ displacements vector and q heat sources. The dot and colon signs

denote scalar product and second order tensor contraction, respectively.

The subscripts e and p denote elastic and plastic components of the strain tensor, respectively, while superscript p denotes states computed for the previous time step in the time integration procedure. The integrals in the above equations are integrated over Ω domain following the finite element methodology. In order to make the development of finite element codes for above formulations as efficient as possible the authors use AceGen (Korelc, 2009a) system for automatic code generation. The system combines symbolic and algebraic systems, problem solving environments and automatic differentiation tools that can be applied to efficiently derive codes for implicit time integration schemes employing consistent tangent operators for primal analyses of nonlinear, transient and path dependent problems. The details how this can be achieved are provided by Korelc (2009b). Furthermore, in this reference it is shown that primal analyses can be extended very efficiently also to the sensitivity analyses that enable application of gradient based algorithms for solution of complex inverse and optimisation problems in science and engineering. One of the important advantages of the symbolic approach is that is that it allows very efficient introduction and modification of constitutive models as well as sensitivity analyses in the context of large strain frictional contact problems Stupkiewicz et al. (2002). For the materials considered in this work the J2 elasto-viscoplastic material model was applied based on the well known Sellars-Tegart expression (Humphreys & Hatherly, 1995) discussed in Section 4.

As an alternative to the fully implicit finite element code generated by AceGen the authors also apply explicit time integration schemes to the coupled equations 2 and 3 as they are implemented in the ELFEN finite element system (ELFEN, 2010).

3.2. Evolution of microstructure during static recrystallization

For the simulations of the microstructure evolution during static recrystallization a cellular automata method was applied. Cellular automata are dynamic systems with local interactions in which space and time are discrete. The space of interest is divided into a regular lattice of cells, and the state of every cell is determined by the states of its neighboring cells, and its previous state through the synchronous application of the transformation rule, which computes the new states of all the cells and could be either deterministic or probabilistic. The CA method for simulating static recrystallization was first introduced by Hesselbarth and Göbel (1991) and has since been applied to simulate a wide range of phenomena in materials science and metallurgy (Hesselbarth & Göbel, 1991; Raabe, 2002; Raabe & Becker, 2000; Kugler & Turk, 2004; 2006; Yazdipour et al., 2007; Madej et al., 2007a; Svyetlichnyy, 2009; 2007; 2010; Madej et al., 2007b; Cvahte, 2010). The simulation procedure adopted here consists of two main steps, i.e. nucleation and growth of recrystallized grains. Static recrystallization proceeds by the formation of dislocation-free regions (with sufficient misorientation for growth) called nuclei and their growth. In the present model the nucleation stage was modelled phenomenologically by defining the nucleation probability p_m and all the cells that are marked as potential nuclei are then tested with this probability. Namely, the cell become a nucleus if

$$p < p_m;\ p \in [0,1],$$

where p is randomly generated number. Determination of the nucleation probability can be very difficult task, since there are still many open questions regarding the nucleation stage of recrystallization (Humphreys & Hatherly, 1995). On the other hand it is known from the theory and from experimental observations that nucleation rate is proportional to stored strain energy, E_D, and inversely proportional to specific surface energy, γ_{GB}. Since nucleation is thermally activated process the expression for nucleation probability has to include the Arrhenius term and thus probability for nucleation can be estimated as

$$p_m \propto E_D \gamma_{GB}^{-1} \exp(-Q_n/RT), \quad \text{or}$$

$$p_m = C_0 \rho \exp(-Q_n/RT), \tag{3}$$

by taking into account that $E_D \propto \rho G b^2$, where ρ is dislocation density, G shear modulus, b the magnitude of the Burger's vector, C_0 is constant, R is the universal gas constant, and Q_n the activation energy for nucleation. Note that similar dependence (3) of probability for nucleation on temperature and stored energy, which was employed in the present model, was also used by the Song et al. (2001; 2002) in their Monte Carlo simulations of static recrystallization in titanium alloys.

In the growth step the states of all recrystallized cells remain unchanged, while a non-recrystallized cell stays non-recrystallized unless there is a recrystallized cell in its neighborhood. If so, the cell is marked as partially recrystallized. It become fully recrystallized when $r_c \geq d_0$, where r_c is the distance parameter and d_0 the size of one cell. It is generally accepted that the driving pressure for grain boundary movements, p, which comes from the stored energy in the deformed matrix, and the velocity, v, of the advancing grain boundary are linearly dependent (Humphreys & Hatherly, 1995), thus

$$v = Mp\,, \tag{4}$$

where M is grain boundary mobility given with (Humphreys & Hatherly, 1995; Frost & Ashby, 1982)

$$M = b\delta D_b (kT)^{-1} \exp(Q_b / RT)\,. \tag{5}$$

Here δ is the characteristic grain-boundary thickness, D_b is the boundary self-diffusion coefficient, Q_b is the boundary-diffusion activation energy and k is Boltzmann's constant. The driving pressure for grain boundary movements depends on the dislocation-density difference, $\Delta\rho$, on both sides of the moving boundary and can be written as (Humphreys & Hatherly, 1995)

$$p = cGb^2 \Delta\rho\,, \tag{6}$$

where G is shear modulus and c is a constant in the order of 0.5. The contribution of capillary pressure arising from boundary curvature was neglected in the present study.

After deformation also static recovery, which can significantly reduce the stored deformation energy before and during recrystallization, takes place. This is especially emphasized in high-stacking-fault-energy metals such as aluminum where dislocation movement is rapid. Static recovery promotes nucleation in the early stages of recrystallization and at the same time decreases the recrystallization rate in its later stages. In the present model a simple model for static recovery was selected (Humphreys & Hatherly, 1995)

$$\dot{\rho} = -k\rho^n\,, \tag{7}$$

where n and k are constants. Since the values of these two constants are not known and their experimental determination is very difficult, we set $n \equiv 1$, and k as a free parameter of the model. The time evolution of the distance parameter of the particular cell, r_c, depends on whether the cell is marked as recrystallized (R), non-recrystallized (NR) or partially recrystallized (PR), and is calculated as

$$r_c^t = \begin{cases} r_c^{t-\Delta t}; & (C \in R) \vee (C \in NR) \\ r_c^{t-\Delta t} + v\Delta t; & (C \in PR) \wedge (v > 0) \end{cases} \tag{8}$$

For simplicity, the current simulations of microstructure evolution were carried out in 2D. The simulation lattice was 1280×800 and Moore neighborhood together with Neumann boundary conditions was used. The size of one cell, d_0, was 4 μm and thus the simulation area corresponds to 5.12 x 3.2 mm in the real dimensions. The time step was defined as $\Delta t = \eta \cdot d_0 / v_{max}$, where v_{max} is the maximal grain boundary velocity from the previous step and η is parameter taken as 0.2. In every nucleation step all the cells are checked if the condition for the cell to become the nucleus is satisfied. If so, then such cell is written in the vector of potential nucleuses. The conditions for creation of potential nucleuses are defined at the beginning of simulation and depend on whether one needs to simulate topologically homogenous or heterogonous nucleation. For topologically homogenous nucleation every non-recrystallized cell becomes potential nucleus, whereas only cells on grain boundaries of initial microstructure or on other prescribed high-energy defects inside grains (e.g., deformation bands, dislocation tangles, sub-grain walls, particles, etc.), which could also act as nucleation sites, are selected for topologically heterogonous nucleation. Of course, in the latter case the initial microstructure must be provided either from experiments or by simulations. Whether we are dealing with a topologically heterogeneous or homogeneous nucleation depends mainly on the ratio between the sizes of microstructural features before and after recrystallization[1] (Kugler & Turk, 2006). Note that topologically homogenous nucleation that has been selected for the present simulations does not necessarily imply homogenous nucleation, since in general nucleation also depends on other parameters, such as temperature, stored energy, orientation gradients, etc., which may be heterogeneously distributed in the material, which

[1] For example, if the ratio between the average grain sizes before and after recrystallization is more than 1:100 like in the present case (compare figures 1b and 10), and grain boundaries are the only topological feature of the initial microstructure, we are dealing with a topologically homogeneous nucleation.

leads to heterogeneous nucleation and consequently to heterogeneous recrystallization.

The initial stored energies for CA simulations of static recrystallization are obtained from FEM simulations. The coupling between both methods consists of extracting and translating the local hot working parameters into dislocation density and its mapping on the CA grid. The temperature of the extruded profile after hot extrusion was obtained by fitting the industrial measurements to the selected function and mapping the results on the CA grid. The coupling between mesoscopic and macroscopic scale and with industrial measurements of temperature that have been employed in the present simulations is schematically shown on figure 3.

metals deformed under hot working conditions. Note that for all testing conditions the steady state stress occurs for strains below 0.1.

The influence of temperature and strain rate on steady state stress was described by the empirical Sellars-Tegart sine-hyperbolic equation which was originally developed for creep and is also widely applied to hot working (Humphreys & Hatherly, 1995):

$$Z = \dot{\varepsilon}\exp(Q_d / RT) = C\sinh^n(\alpha\sigma), \qquad (9)$$

where Q_d is the activation energy for deformation, n, α, C are materials constants, and Z is the Zener–Hollomon parameter. The activation energies as well as other constants in this equation (9) taking into

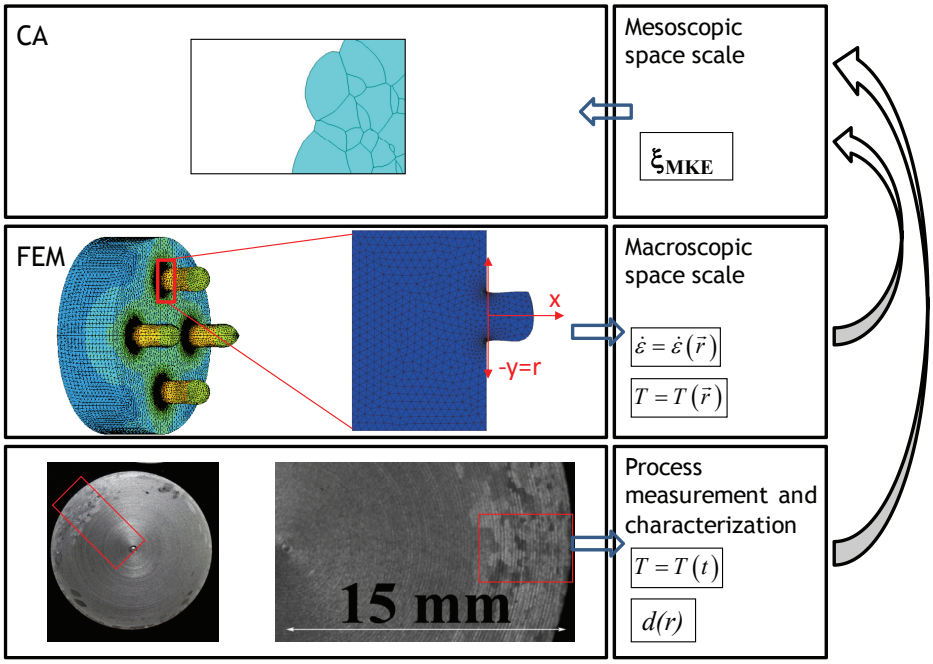

Fig. 3. *CA model for microstructure evolution coupled with FEM model for simulations of extrusion and industrial measurement of temperature of surface of the extruded profile as a function of time after extrusion.*

4. RESULTS AND DISCUSION

In order to obtain the flow curves and dependences between steady state stress, strain rate and temperature for the alloy AA6262 that have been used in numerical simulations, a series of compression tests were carried out for temperatures between 470°C and 570°C, and strain rates between 0.01s^{-1} and 10s^{-1}. Typical stress-strain curves are shown in figure 4a. The flow curves for all tested temperatures and strain rates initially exhibit an intensive work hardening until dynamic recovery balances strain hardening, and a steady state is reached. As expected the flow stress decreases with decreasing strain rate and increasing temperature, which is typical for

account the errors of the steady state flow stresses were determined using the procedure described in Kugler et al. (2004). The activation energy amounts 211 kJ/mol, which is close to the values reported in the literature for AA6262 alloy (Sheppard, 1990). All determined parameters of sine-hyperbolic equation are given in table 3. The comparison between the calculated and measured values of the steady-state stresses is shown in figure 4b. Other materials parameters for numerical simulations such as density, Yung, bulk and shear modulus, Poisson's ratio, specific heat, thermal conductivity, etc., and their temperature dependence have been determined using JmatPro commercial software which enables calculations of wide range of materials properties for

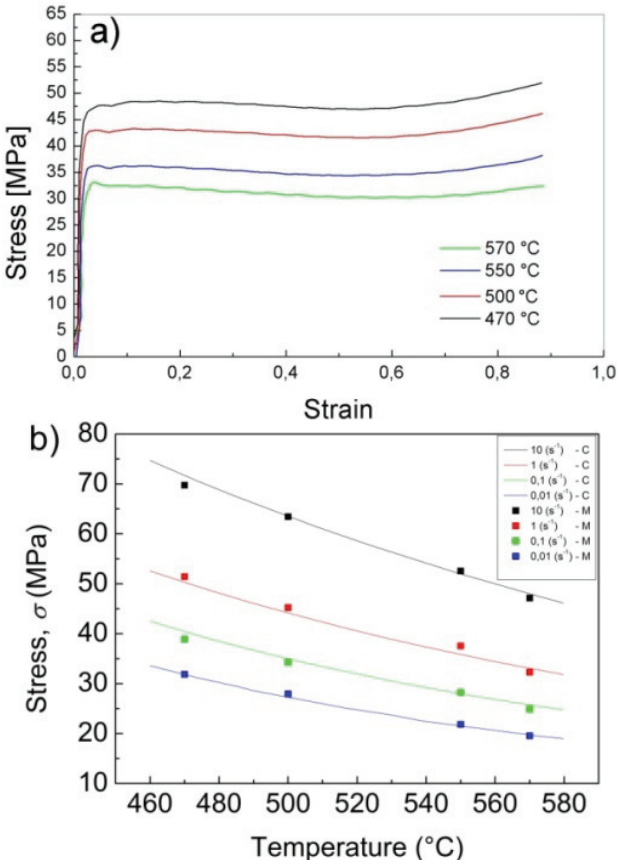

Fig. 4. *Stress-strain curves for different temperatures and strain rate of 1 s^{-1} (a).Comparison between measured and calculated dependence of steady state flow stress on temperature for various strain rates (b).*

multi-components alloys used in industrial practice (Saunders et al., 2004,). During the extrusion testing in industry, a series of measurements of processing parameters has been conducted that have been used for calibrations of the numerical model. The most important are the speed of the extrusion ram, time which is needed by the extruded material to reach the quenching facilities, and various temperatures on the entire processing chain. The obtained speeds of the ram which have been used in numerical simulations of extrusion were 5.5, 9.9, 12.8, 15 and 18 mm/s and the corresponding times that elapse between the bar step out of the extrusion die and reaches the quenching section were 45, 25, 19, 16 and 14 s. Temperature field for the entire geometry of the extruded billet for the ram speed of 9.9 mm/s obtained with FEM simulations of extrusion is shown on figure 5a, while temperature and strain rates in cross section in direction of extrusion is shown on figures 5b and 5c, respectively.

Here it should be mentioned that during hot deformation of high stacking fault energy materials such as Al alloys, beside dynamic recovery, also continuous dynamic recrystallization and geometric

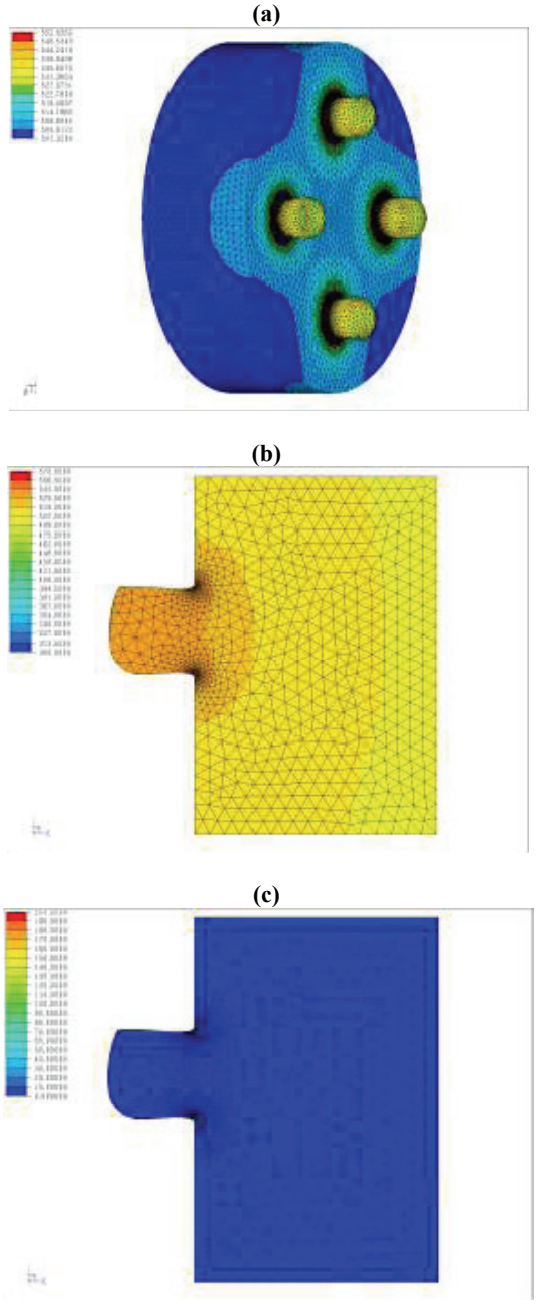

Fig. 5. *Results of the FEM simulations of extrusion: temperature field for entire geometry (a), temperature (b) and strain rate (c) in cross section in direction of extrusion of the extruded profile.*

dynamic recrystallization have been observed. During continuous dynamic recrystallization the misorientation across some low-angle grain boundaries increases to such extend (e.g. >15°) that they transform to high-angle grain boundaries. These newly formed high-angle grain boundaries then very slowly migrate and reduce the dislocation density which consequently leads to softening of material and grain refinement (Gourdet & Montheillet, 2003; DePari Jr. & Misiolek, 2008). On the other hand geometrical dynamic recrystallization is characterized by increased flattening of grains due to straining, which finally leads to pinching-off of portions

of grains and consequently to grain refinement. Since these two mechanism become more pronounced at large strains ($\varepsilon >> 1$) they have been neglected in the present study where maximal obtained strains were $\varepsilon < 1$ (see figure 6a). As can be seen from figure 4a, for $\varepsilon < 1$ no additional softening can be observed. Furthermore the inspection of microstructures of material that have been extruded with the lowest ram speed, where static recrystallization was not observed, revealed elongated grains with no indication on geometric dynamic recrystallization.

In order to obtain values for the initial condition for simulations of evolution of microstructure during static recrystallization after hot extrusion and to establish the coupling between FEM and CA simulations the dislocation density of the extruded bar for the moment when straining stops have been estimated using expression that relates the high-temperature flow stress to the density of dislocations (Humphreys & Hatherly, 1995)

$$\sigma = \sigma_0 + c_1 MGb\sqrt{\rho}, \qquad (10)$$

where σ_0 is mechanical threshold stress, c_1 is a dislocation-interaction term, which is between 0.5 and 1.0 for most metals, and M is Taylor factor. It should be mentioned here that dislocation density could be obtained by employing a crystal plasticity finite-element simulation of extrusion as has been done by Raabe and Becker (2000), but such approach would be very difficult to implement in our case, where real industrial process of hot extrusion is simulated. Namely, the crystal plasticity approach is computationally very expensive and therefore less expensive estimation of dislocation density using equation 10 was employed in the present work. Figure 6a shows the true strain as a function of distance from the center of the extruded profile, r, for the cross-section where the bar leaves the extrusion die, obtained with FEM simulations of extrusion. Referring to this figure it can be seen that the true strain is well above 0.2 for the areas below the surface of the bar where static recrystallization occurs at all testing conditions employed in the present work. Therefore in these areas the steady state stress for the given thermo-mechanical conditions, i.e. temperature and strain rate, have been established (see figure 4a). By knowing the strain rates and temperatures profiles across the cross-section of the bar the dislocation densities can be estimated by combining equations 9 and 10 as

$$\rho(\vec{r}) = \left(\frac{\sigma_{ss}(\dot{\varepsilon}(\vec{r}), T(\vec{r}))}{c_1 GbM} \right)^2 \qquad (11)$$

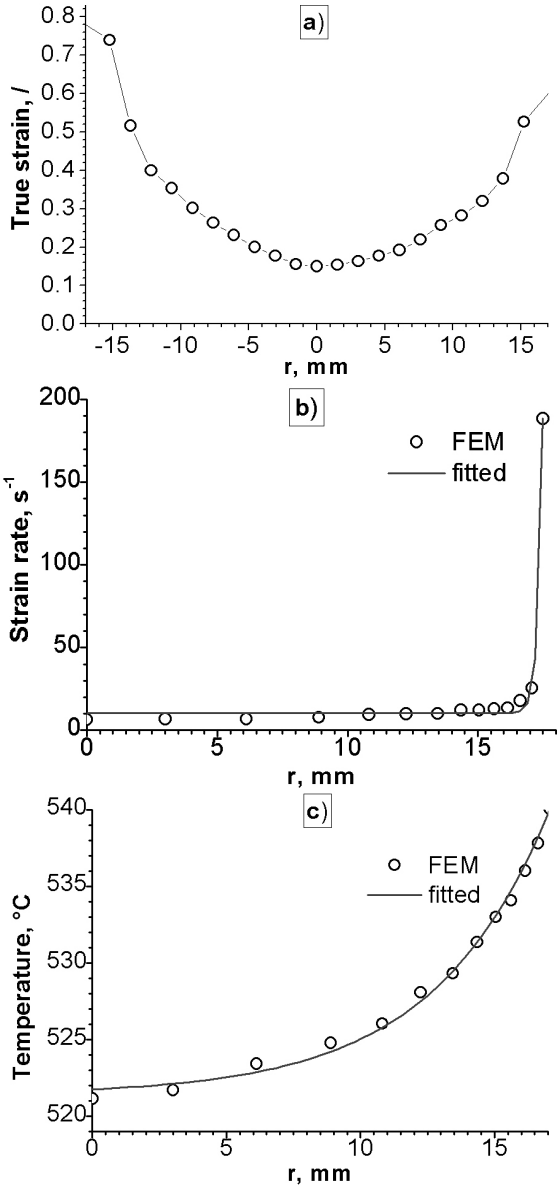

Fig. 6. *True strain (a), strain rate (a), and temperature (b) as a function of distance from the center of the bar, r, of the extruded profile, for the moment when the bar leave the extrusion die, obtained with FEM simulations of extrusion for the ram speed of 12.4 mm/s.*

Strain rate and temperature as a function of r obtained with FEM simulations for the ram speed of 12.4 mm/s are shown on figures 6b and 6c, respectively. In order to obtain continuous dependences' on r the values of these two parameters given in integration points of FEM were fitted to exponential functions.

Figure 7a shows typical temperature dependence on time for the bar that was cooled on the air after hot extrusion and was obtained by the industrial measurements. As can be seen, this temperature

varies linearly for the time intervals which are relevant for our simulations of evolution of microstructure. Thus

$$T(t) = a_0 + a_1 t\,, \qquad (12)$$

where a_0 and a_1 are given in table 2 for all ram speeds considered in the present study and were obtained by fitting the measured temperatures to (12).

Table 2. *The parameters obtained by fitting measured temperatures to straight line.*

Ram speed [mm/s]	5.5	9.9	12.8	15	18
a_0 [°C]	540	547	553	556	560
a_1 [°C/s]	-0.18	-0.18	-0.18	-0.18	-0.18

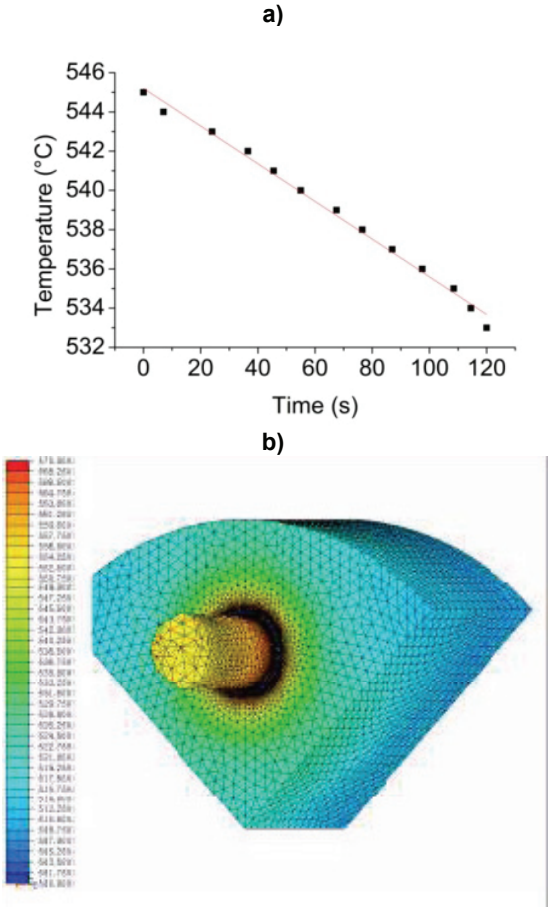

Fig. 7. *Measured surface temperature of extruded profile as a function of time after extrusion (a), and temperature field obtained by FEM simulation (b).*

Figure 7b shows temperature field obtained by FEM simulation. It was observed that when the bar is cooled on the air after hot extrusion, the temperature gradient within the area where statistic recrystallization occurs very quickly becomes negligible. Therefore the temperature variation during the simulations of the evolution of microstructure was described using equation 12 neglecting its spatial variations.

Material constants used in the present simulations of the evolution of microstructure during static recrystallization are collected in table 3. The constants Q_n and C_0 for nucleation probability (3) and parameter k which appears in expression for static recovery (7) are very difficult to determine experimentally. Therefore they have been taken as a free parameters of the model and were determined firstly by comparing the simulated and real final microstructures for the profile obtained by employing the ram speed of 12.8 mm/s and has not been quenched after extrusion, and secondly by assuring that results of simulations agree with experimental results where for the lowest ram speed of 5.5 mm/s no nucleation of new grains was observed in the microstructure. Taking into account these conditions the free parameters were found by trial and error calibration procedure and are also given in table 3. Note that parameter k also partially compensate the errors that has been done by the simplifying assumptions for determining the dislocation density at the moment when straining stops.

Table 3. *The values of material parameters used in simulations obtained experimentally or taken from (Frost & Ashby, 1982).*

Q_b [kJ/mol]	δD_b [$m^3 s^{-1}$]	G [Pa]	b [m]	Q_n [kJ/mol]	C_o[m^2]
120	$5.0\ 10^{-14}$	$1.84\ 10^{10}$	$2.86\ 10^{-10}$	102	$7.0\ 10^{-6}$
Q_d [kJ/mol]	n [/]	A [s^{-1}]	α [Mpa^{-1}]	k [s^{-1}]	M [/]
211	7.94	$5.0\ 10^{13}$	0.0226	0.02	3

Figure 8 shows the results of simulation of evolution of microstructure for ram speed of 12 mm/s. It can be seen that in the incipient stages of recrystallization spatial distribution of nuclei is very inhomogeneous as they are concentrated near the surface. This is an expected result since the stored energy is the highest near the surface. Higher density of nuclei near the surface results in finer microstructure, which becomes coarser with increasing distance from the surface. It can also be observed that nucleation rate is decreasing with time. Again this is expected result due to decreasing temperature and static recovery which decreases deformation stored energy. Decreasing temperature and stored energy result in lower probability for nucleation. Additionally as recrystallization proceeds less material is available for nucleation of new grains. It can be seen from those figures

that grain growth rate is decreasing with time due to decreasing grain boundary mobility and lower driving force in the areas away from the surface as a consequence of lower stored energy from deformation. Namely, nucleation involves randomness and lower number of nucleuses results in higher scatter of results.

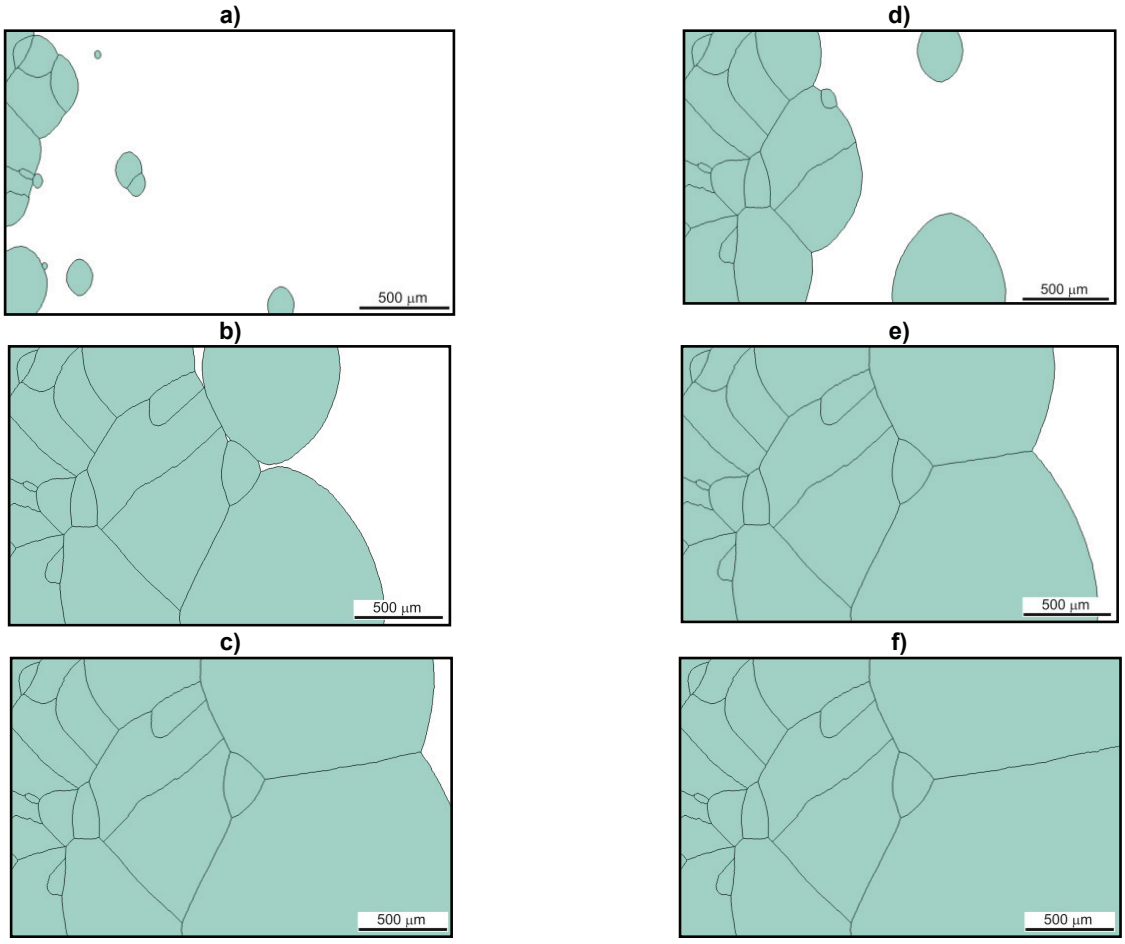

Fig. 8. *Evolution of microstructure during cooling of extruded profile obtained by CA simulations for ram speed of 12 mm/s after: 20 s (a), 40 s (b), 60 s (c), 80 s (d), 100 s (e), and after 130 s (f). Surface of the profile is on the left side of the pictures.*

Very important technological parameter that influences the quality of the extruded profiles is the depth of the recrystallized surface zone which can occurs during industrial production before the profile reaches the quenching section. Therefore simulations of evolution of microstructure have been conducted for all the ram speeds that were employed in the present industrial research. The results are shown on figure 9 where comparison between measured and simulated depth of the recrystallized zone as a function of ram speed is given. Very good agreement was obtained. In order to determine the standard deviations of the results 10 simulations for every ram speed have been performed.

As can be seen the difference between industrial measurements and simulated results increases with decreasing depth of the transition zone. These can be attributed to the number of grains which are present in microstructure at the moment of quenching.

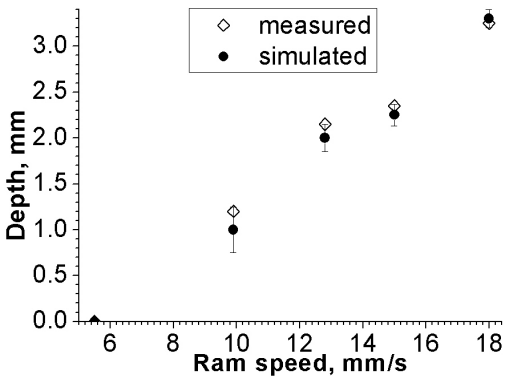

Fig. 9. *Comparison between measurements and simulations of evolution of microstructure: depth of the recrystallized zone as a function of ram speed. Error bars correspond to standard deviations.*

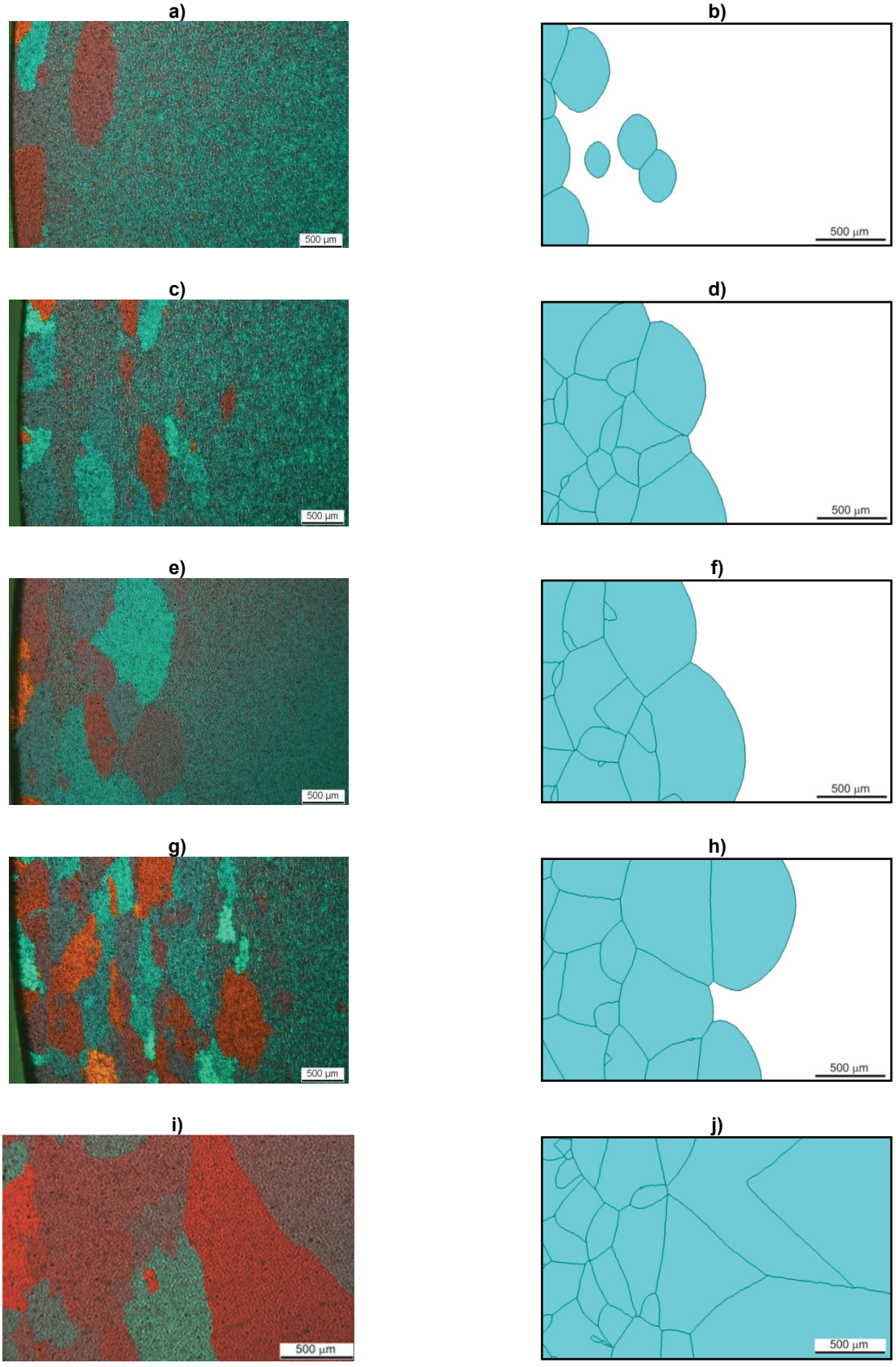

Fig. 10. *Comparison of real and simulated microstructures for ram speed of 9.9 mm/s with quenching after 25 s (a) and (b), ram speed of 12.8 mm/s with quenching after 19 s (c) and (d), ram speed of 15 mm/s with quenching after 16 s (e) and (f), ram speed of 18 mm/s with quenching after 14 s (g) and (h),and ram speed of 12.8 mm/s with quenching after 190 s (i) and (j).*

Note that it is straightforward to include additional state variables into cellular automata model, but in the present work textures have not been considered since they have not been experimentally determined. Nevertheless, the visual inspection of the shapes of recrystallized grains in the microstructure of extruded rods shows that grains are slightly elongated in the direction parallel to the surface of the rods. This is the consequence of the deformation texture, which has not been taken into account in the present study. Namely recrystallization fronts oriented in preferential direction can be several times faster than those oriented in different directions (Humphreys & Hatherly, 1995). In order to take this into account, at least to some degree, the pre-exponential factor in equation 5 was artificially multiplied by the factor of 0.5 for the movement of recrystallization front in the direction perpendicular to surface of the rod.

In figure 10 the comparison of microstructures for the various ram speeds at the moment the profiles are water quenched during their industrial production. The left and right columns of this figure show the microstructures obtained by metallography and simulations, respectively. Note that microstructures for the lowest ram speed of 5.5 mm/s are not shown here since in this case no recrystallization was observed within time interval before quenching, neither for industrial, nor for simulated microstructures. Furthermore, in order to reveal the recrystallization process for longer times, the water quenching after hot extrusion have been omitted for some profiles. One such example is shown in figures 10i and 10j where real microstructure of the profile for the ram speed of 12.8 mm/s after 190 s is compared with simulated one. As can be seen from micrographs in figure 10, the essential feature of the heterogeneity of the real recrystallized microstructures have been captured with our model: the smallest grains are lying close to the surface and their sizes increase with their distance from the surface. Similarly sufficient agreements were also obtained for mean grain sizes. Some discrepancies are observed only for the highest ram speed of 18 mm/s. Namely, a few small grains were observed in industrial samples also at larger distance from the surface and thus observed mean grain size in the real material is slightly lower than in the simulated microstructure.

5. CONCLUSIONS

In the paper an approach for prediction of statically recrystallized microstructure during hot extrusion of aluminum alloys is presented. The mesoscopic recrystallization model is based on CA method and is coupled with macroscopic FEM model for simulation of extrusion. Within the framework of the present study the comprehensive experimental work both in laboratory and in industry has been conducted. Based on these results, detailed simulations were employed aiming to predict the influence of the ram speed on the evolution of microstructure and especially on the depth of the surface recrystallization zone. From our simulations the following conclusions can be drawn: (1) despite of many simplifying assumptions, our model can capture the essential features of the heterogeneous static recrystallization observed in aluminum alloys after hot extrusion, (2) the predicted depth of the recrystallized zone under the surface of the extruded profiles, agree very well with the results of industrial measurements on AA6262 alloy for all the ram speeds employed in the present work, and (3) the results of simulations of evolution of microstructure show a good agreement with the results of optical micrographs of the profiles that were taken from industrial production.

REFERENCES

Cvahte, P., 2010, *Coupled thermo-mechanical and metallurgical processes during extrusion of Al-alloys*, Ph.D. Thesis, University of Ljubljana, Ljubljana.

DePari, Jr. L., Misiolek, W. Z., 2008, Theoretical predictions and experimental verification of surface grain structure evolution for AA6061 during hot rolling, *Acta Mater.*, 56, 6174-6185.

ELFEN Finite Element System – Specification document. Available online from: http://www.rockfield.co.uk/products.htm (last accessed: 2.12.2010).

Frost, H.J., Ashby, M.F., 1982, *Deformation-Mechanisms Maps*, Pergamon, Oxford.

Gourdet, S., Montheillet, F., 2003, A model of continuous dynamic recrystallization, *Acta Mater.*, 53, 2685-2699.

Hesselbarth, H.W., Göbel, I.R., 1991, Simulation of recrystallization by cellular automata, *Acta Metall. Mater.*, 39, 2135-2143.

Humphreys, F.J., Hatherly, M., 1995, *Recrystallization and Related Annealing Phenomena*, Pergamon, New York.

Korelc, J., 2009b, Automation of primal and sensitivity analysis of transient coupled problems, *Comp. Mech.*, 44, 631-649.

Korelc, J., 2009a, AceGen and AceFEM user manuals. Available online from: http://www.fgg.uni-lj.si/Symech/ (last accessed: 2.12.2010).

Kugler, G., Knap, M., Palkowski, H., Turk, R., 2004, Estimation of activation energy for calculating the hot workability properties of metals, *Metalurgija*, 43/4, 267-272.

Kugler, G., Turk, R., 2004, Modeling the dynamic recrystallization under multi-stage hot deformation, *Acta Mater.*, 52, 4659-4668.

Kugler, G., Turk, R., 2006, Study of the influence of initial microstructure topology on the kinetic of static recrystallization using cellular automata model, *Comp. Mater. Sci.*, 37, 284-291.

Madej, L., Hodgson, P.D., Pietrzyk, M., 2007b, The validation of a multiscale rheological model of discontinuous phenomena during metal rolling, *Comp. Mater. Sci.*, 41, 236-241.

Madej, L., Szeliga, D., Kuziak, R., Pietrzyk, M., 2007a, Physical and numerical modelling of forging accounting for exploitation properties of products, *Comp. Methods. Mater. Sci.*, 7, 397-405.

Peng, Z., Sheppard, T., 2004, Individual influence of forming parameters on surface recrystallization during aluminium extrusion, *Modelling Simul. Mater. Sci. Eng.*, 12, 43-58.

Raabe, D., 2002, Cellular automata in materials science with particular reference to recrystallization simulation, *Ann. Rev. Mater. Res.*, 32, 53-76.

Raabe, D., Becker, R. C., 2000, Coupling of a crystal plasticity finite element model with a probabilistic cellular automaton for simulating primary static recrystallization in aluminium, *Modell. Simu. Mater. Sci. Eng.*, 8, 445-462.

Saunders, N., Guo, Z., Miodownik, A. P., Schillé, J-Ph., 2004, Modelling Materials Properties and Behaviour of Multicomponent Alloys, *22nd CAD-FEM User's Meeting, International Congress on FEM Technology*, Dresden, Germany, 1-8.

Sheppard, T., 1999, *Extrusion of Aluminium Alloys*, Kluwer Academic Publishers, Dordrecht.

Song, X., Rettenmayr M., 2002, Modelling study on recrystallization, recovery and their temperature dependence in inhomogeneously deformed materials, *Mater. Sci. Eng. A*, 332A, 153-160.

Song, X., Rettenmayr, M., Mueler, C., Exner, H., 2001, Modeling of recrystallization after inhomogeneous deformation, *Metall. Mater. Trans. A*, 32A, 2199-2206.

Stupkiewicz, S., Korelc, J., Dutko, M., Rodič, T., 2002, Shape sensitivity analysis of large deformation frictional contact problems, *Comp. Meth. Appl. Mech. Engng.*, 191, 3555-3581.

Svyetlichnyy, D., 2009, Modeling of microstructure evolution during the rolling by using cellular automata, *Comp. Methods. Mater. Sci.*, 9, 256-263.

Svyetlichnyy, D., 2010, Modelling of the microstructure: From classical cellular automata approach to the frontal one, *Comp. Mater. Sci.*, (in print).

Svyetlichnyy, D.S., 2007, Some aspects which deny a use of 2D cellular automata for modelling of recrystallization, *Comp. Methods. Mater. Sci.*, 7, 175-181.

Yazdipour, N., Davies, C.J., Hodgson, P.D., 2007, Simulation of dynamic recrystallization using random grid cellular automata, *Comp. Methods. Mater. Sci.*, 7, 168-174.

PRZEWIDYWANIE MIKROSTRUKTURY PO STATYCZNEJ REKRYSTALIZACJI W PROCESIE WYCISKANIA ALUMINIUM

Streszczenie

Aby przewidywać rozwój mikrostruktury stopów aluminium w procesie wyciskania opracowano numeryczny model wykorzystujący metodę automatów komórkowych (ang. Cellular automata - CA), który połączono z metodą elementów skończonych (ang finite element method - FEM). Głównym celem połączonych modeli FEM-CA jest przeprowadzenie numerycznych symulacji rozrostu ziarna w warstwie przypowierzchniowej wyciskanego pręta. Taki rozrost jest obserwowany w warunkach przemysłowych po wyciskaniu przed rozpoczęciem chłodzenia wyrobu. Wyniki numerycznych symulacji wykazują dobrą zgodność z pomiarami za pomocą mikroskopii optycznej dla prętów pobranych z prób przemysłowych. Przeprowadzone badania wykazują, że modelowanie numeryczne może być z powodzeniem zastosowane do symulacji skomplikowanych zjawisk cieplno-mechanicznych i metalurgicznych podczas wyciskania na gorąco.

Received: September 26, 2010
Received in a revised form: December 1, 2010
Accepted: December 2, 2010